Aerosol and Air Quality Research, 16: 1638–1650, 2016

ISSN: 1680-8584 print / 2071-1409 online
doi: 10.4209/aaqr.2015.02.0076

Bonding Structure and Mineral Analysis of Size Resolved Atmospheric Particles nearby Steelmaking Industrial Sites in Australia

Kazi Mohiuddin[1,2*], Vladimir Strezov[1], Peter F. Nelson[1], Tim Evans[1]

[1] *Department of Environmental Sciences, Faculty of Science and Engineering, Macquarie University, Sydney, Australia*
[2] *Department of Civil Engineering, Khulna University of Engineering & Technology, Khulna 9203, Bangladesh*

ABSTRACT

Comprehensive understanding of organic and inorganic compounds in atmospheric particles of different size fractions ranging from coarse to ultrafine is essential for assessment of the impact of particles on the radiation balance. In this work the size resolved atmospheric particles were collected in the vicinity of three iron and steelmaking sites and one urban background site in Australia using an eight staged micro orifice uniform deposit impactor (MOUDI) sampler. The sampled particles were assessed using FTIR technique to determine the dominant functional groups, and XRD technique for determining the mineral content of the inorganic compounds. This study revealed variable distributions between and among bonding groups in urban and industrial areas. The hydroxyl (–OH) group (in alcohol compounds, surface OH on crystals, salt hydrate), aliphatic carbon ($–CH_2$) group (in methylene compounds, n-alkane), carbonyl (–CO) group (in acid halide, aryl carbonate, ketone, conjugated ketone), and amino ($–NH_2$) group (in primary amino compounds such as n-butylamine) in atmospheric particles were identified and most likely originated from combustion processes (industrial, transport, and domestic), sea spray, long range transport particles, and secondary organic particles sources nearby industrial and urban areas. Hematite mineral in the inorganic fraction of the atmospheric particles was found predominantly in the vicinity of the iron and steelmaking industries, which most likely originates from raw materials handling and process emissions.

Keywords: Atmospheric particles; Steelworks; FTIR; XRD; Hematite.

INTRODUCTION

Atmospheric particles released from industrial sectors are posing significant challenges to the surrounding air quality and the climate change. Industrial atmospheric particles are complex and heterogeneous and may contain numerous organic and inorganic compounds, which vary according to the particle size fraction. The level of toxicity also increases with the decrease of particle size, especially for fine and ultrafine particles (Braakhuis *et al.*, 2014). Most of the particle characterisation studies are limited to mass and elemental concentration of the PM_{10} and $PM_{2.5}$ particle size range (Hibberd *et al.*, 2013; Cohen *et al.*, 2014; Karlson *et al.*, 2014) and few studies have been performed for elemental composition of size resolved atmospheric particles (Radhi *et al.*, 2010; Mohiuddin *et al.*, 2014a, b). Although elemental compositions of particles provide the assessment of environmental exposure and associated risks, further analysis on bonding structure and mineral content is required, especially for the impact assessment of particles on radiative forcing.

Organic compounds (carbonaceous and nitrogenous molecules) in atmospheric particles can have negative impacts on human health (Dockery *et al.*, 1993; Alcock, 2003; Shah and Balkhair, 2011), ecosystem (Cupr *et al.*, 2013) and the radiation balance (Hallquist *et al.*, 2009; Ehn *et al.*, 2014). These compounds can be generated from both natural (secondary organic particles from biogenic sources) and anthropogenic (industrial process, vehicle exhaust, wood heaters) sources. Organic compounds can be examined using elemental analysis or gas chromatography–mass spectrometry (GC-MS), however, about hundred thousand acyclic possible structures can be arranged for the same organic compound due to the diversity of carbon bonding (Roos, 1997). The behaviour of organic compounds also depends on the types of bonding structures. These structural bonding properties of both organic and inorganic compounds in atmospheric particles can be identified and semi-quantified using Fourier Transform Infra-Red (FTIR) technique (Allen *et al.*, 1994; Maria *et al.*, 2002; Ghauch *et al.*, 2006). There are many studies focused on bonding structure in PM_{10} and $PM_{2.5}$ using FTIR method (Ghauch *et al.*, 2006; Coury and Dillner, 2008, 2009), however, unregulated submicron (PM_1) and ultrafine particles ($PM_{0.1}$) are potentially the most hazardous.

* Corresponding author.
Tel.: +880 41 769 471 ext. 225; Fax: +880 41 774 780
E-mail address: kzmohiuddin@gmail.com

This study is the first attempt to analyse the bonding structure and their distribution in size resolved atmospheric particles, including particles within the PM_1 and $PM_{0.1}$ size range, collected nearby Australian blast furnace and electric arc furnace steelworks using the FTIR technique.

Inorganic compounds in atmospheric particles can be constituted of both amorphous and crystalline materials. The elemental composition study of inorganic compounds in atmospheric particles can only provide the total elemental content, which may also originate from amorphous and/or crystalline materials. For example, total iron content in atmospheric particles can be contributed from amorphous metals and crystalline iron minerals, such as hematite, goethite, and magnetite. However, the behaviour of inorganic compounds is highly dependent on mineral phases (Calvo *et al.*, 2013; Reynolds *et al.*, 2014). A variety of minerals could be identified and semi-quantified by examining the unique characteristics (diffracted X-ray beam by crystalline atoms) of crystalline phases in atmospheric particles, which can originate from both natural and anthropogenic sources. Study of iron minerals in industrial atmospheric particles is essential as the radiative forcing characteristics (both direct radiative impact and role as a cloud nuclei) of atmospheric particles is highly dependent on the iron mineral content of atmospheric particles (Claquin *et al.*, 1999; Sokolik *et al.*, 1999; Meland *et al.*, 2011; Journet *et al.*, 2014). Some studies focused on mineral analysis of bulk samples of atmospheric particles (TSP, PM_{10}) (Ohmsen, 2004a, b; Lu *et al.*, 2007; Hleis *et al.*, 2013), however mineral types and quantity can vary significantly with different size fractions of atmospheric particles. The process efficiency and environmental performance of iron and steelmaking industries are also dependent on emission of crystalline minerals generated from fugitive (raw materials handling) and point sources of high temperature processing plants, such as blast furnace, basic oxygen furnace and electric arc furnace, because releasing these minerals at any stage of the steelmaking process could affect the production performance. Hence, it is essential to examine the mineral content of size resolved atmospheric particles in the vicinity of Australian iron and steelmaking industries using X-Ray Diffraction (XRD) technique.

This study was devoted to analyse the bonding structures of organic compounds and the mineral contents of inorganic compounds, including their distribution in size resolved atmospheric particles. The Fourier Transform Infra-Red (FTIR) and X-Ray Diffraction (XRD) analysis were performed for ten different particle size ranges collected from three Australian industrial sites in the vicinity of iron and steelmaking industries and one urban background site. The outcome of this study will provide improved understanding of organic and inorganic compounds in atmospheric particles, and their importance on the radiative forcing of atmospheric particles.

MATERIALS AND METHODS

Sampling Details

Three industrial sites, highly influenced by iron and steel processing industries, and one background site, where little or no industrial influence is expected, were selected to sample the size resolved atmospheric particles in a sampling protocol and for meteorological conditions described previously (Mohiuddin *et al.*, 2014a, b). Fig. 1 shows the locations of all sampling sites. Four sets of samples (ten samples per set) were selected for the FTIR and XRD analysis. Cringila (CR) site (34.4702°S, 150.8728°E) was located in the residential area in New South Wales (NSW) (about 0.5 km away from the ocean) with highly industrial influence in surrounding areas including the Wollongong integrated blast furnace – basic oxygen furnace (BF-BOF) steelworks. Whyalla (WH) site (33.0360°S, 137.5861°E) was located in the residential area in South Australia (about 0.5 km from the long bay and 300 km away from the ocean), and in proximity to the Whyalla integrated BF-BOF steelworks. CR and WH steelworks have the same integrated BF-BOF process of iron and steel production with an exception of the pellet plant at WH steelworks instead of the sinter plant at the CR steelworks. Rooty Hill (RT) site (33.7669°S, 150.8484°E) in NSW was located in the industrial area (about 40 km away from the ocean) nearby the electric arc furnace (EAF) steelmaking plant. The background Macquarie Park (MQ) site (33.7653°S, 151.1176°E) in NSW was located near the Macquarie University sports field surrounded by mainly residential areas (about 20 km away from the ocean). An eight staged Micro Orifice Uniform Deposit Impactor (MOUDI) sampler with Teflon substrate was deployed in the sampling sites to collect the atmospheric particles for at least 24 hrs sampling duration. Mass concentration ($\mu g\ m^{-3}$) of sampled particles at each stage of S0 to SP is shown in Table 1. Further analysis regarding mass and elemental distribution at CR, RT, WH, and MQ sites was found elsewhere (Mohiuddin *et al.*, 2014a, b).

FTIR Analysis

Attenuated Total Reflectance (ATR) technique equipped with ZnSe-Diamond crystal was applied using Nicolet 6700 series Fourier Transform Infra-Red (FTIR) spectrometer to analyse the collected atmospheric particles. 32 scans with 4 cm^{-1} spectral resolution over the range of 4000–500 cm^{-1} were used to prepare the FTIR spectra for the atmospheric particle samples. The blank Teflon substrate was also tested by FTIR technique to confirm the Teflon bond structure and eliminate the overlapping spectra with the particle samples. During the sampling campaign, the atmospheric particles were deposited onto the surface of the Teflon substrates. Small portions in thickness of the Teflon substrate were subjected to the FTIR scan. IR beam (1 mm diameter) was passed through particle samples collected on Teflon filters to acquire FTIR scans. It was difficult to subtract the blank Teflon spectra from the Teflon containing the particle samples, as the IR transmittance through particle samples depends on the thickness of the samples under the FTIR investigation. For this reason, the Teflon spectral peaks were excluded from bonding structure analysis of the atmospheric particle samples. The blank Teflon spectra had strong peaks at 1203.6, 553.5, 505.1 cm^{-1} position and bonding structure was matched with the reference Teflon structure [n(–CF_2–)].

Fig. 1. Map of the sampling sites.

Table 1. Mass concentration (μg m^{-3}) of sampled particles at each stage of S0 to SP.

	S0	S1	S2	S3	S4	S5	S6	S7	S8	SP
CR	1.4	2.4	4.0	5.1	2.8	1.8	1.4	1.6	2.6	1.7
RT	3.8	2.3	2.6	3.5	2.2	1.2	0.3	1.3	1.6	0.2
WH	3.2	5.8	4.6	4.8	4.7	1.6	0.9	0.9	1.0	2.0
MQ	0.5	0.9	0.6	0.9	0.8	1.4	0.7	1.4	1.9	1.7

The Omnic spectra software was used to perform the FTIR scan analysis, including baseline corrections, spectra normalisation and peak integration.

XRD Analysis

The atmospheric particle samples on Teflon substrate were examined for mineralogical composition using X-Ray Diffractometry (XRD). The Teflon substrate was placed on a Si-crystal low background holder to avoid the diffraction peaks generated from aluminium based sample holder. PANalytical X'Pert Pro MPD diffractometer was used to the settings on the sample stage (reflection-transmission spinner), Cu Kα radiation, X'Celerator detector, Bragg Brentano geometry, scan range (18.5–80° 2Θ), generator (40 mA, 45 kV), scan type (continuous), divergence slit type (fixed), divergence slit size (1°), and a high resolution scan using step size of 0.02 2Θ with scan per step of 200 s. 20 mm square beam was used for XRD analysis to acquire XRD scans. Mineral identification and semi-quantification was performed using PANalytical's Highscore Plus software v2.2.4, coupled with ICDD PDF2 and PAN-ICSD mineral databases. The systematic Reitveld refinement technique was applied to identifying minerals using Highscore Plus software.

RESULTS AND DISCUSSION

FTIR Analysis

The spectra of the size resolved atmospheric particles collected from CR, RT, WH, and MQ sites are shown in Fig. 2. The qualitative absorbance frequencies in the coarse, fine, intermodal and submicron size particles at all studied sites are presented in Table 2. The interpretation of the spectra was limited to the selected organic absorbance groups as mentioned below.

Aliphatic Carbon (–CH_2) Group

The aliphatic carbon molecules can constitute of –CH_3, –CH_2, and –CH carbon bonds which may include n-alkanes, branched alkanes, carbonyl containing molecules, alkanes and aromatics aliphatic substituents (Roos, 1997). The characteristic IR spectra of aliphatic carbon bonds occur in the region of 2850–3000 cm^{-1}. The absorption at 2918 and

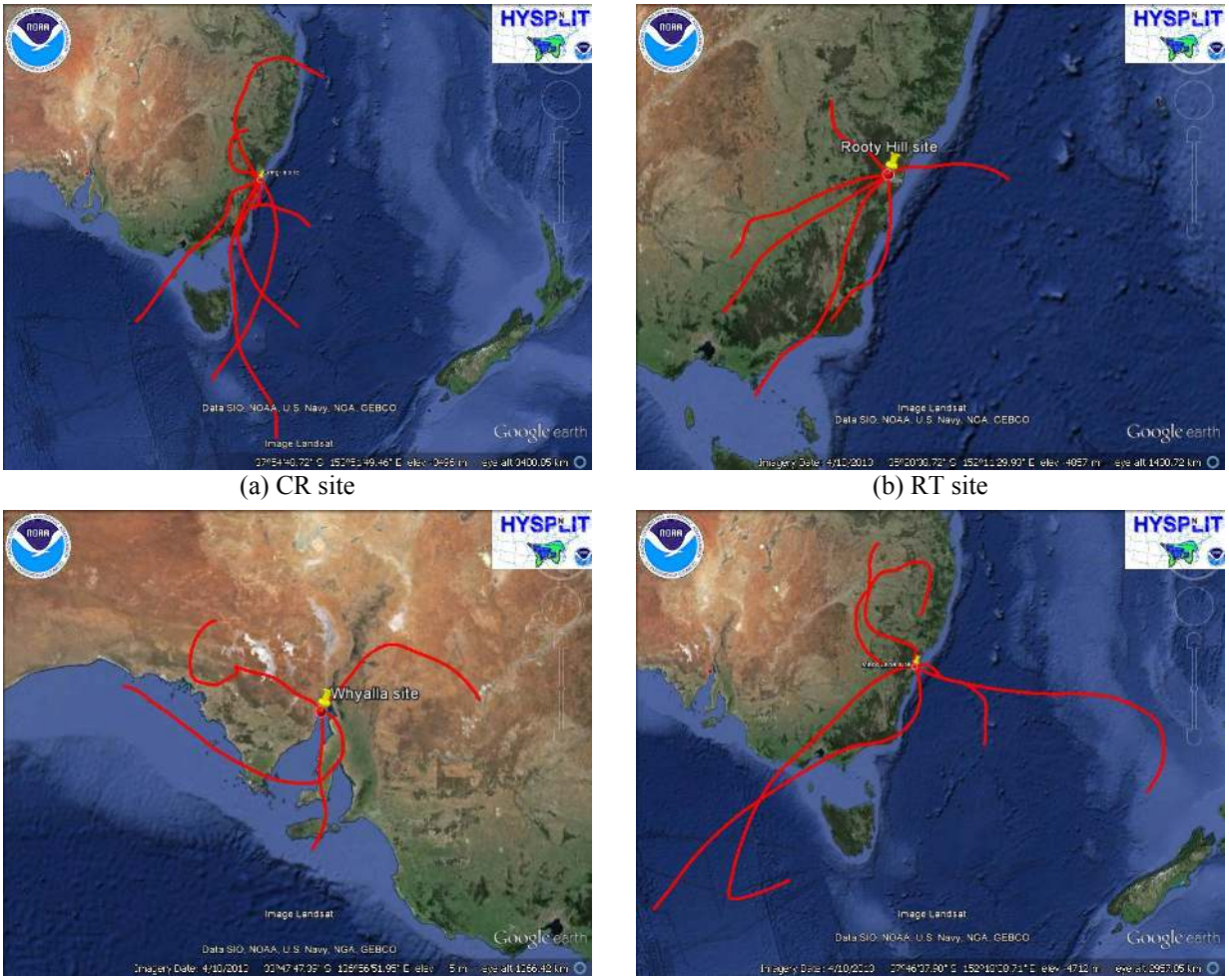

(a) CR site (b) RT site

(c) WH site (d) MQ site

Fig. 2. HYSPLIT back trajectories of sampling sites (CR, RT, WH, & MQ sites) during sampling period.

Table 2. Absorbance observed in the FTIR spectra of air particles.

Functionality		Absorption frequencies (cm^{-1})	Sampling site	Presence in air particle samples			
				Coarse > 2.5 µm*	Intermodal 1–2.5 µm**	Submicron 0.18–1 µm	Ultrafine < 0.18 µm
$–CH_2$	Aliphatic carbons	2850–3000, 1410	CR	H	H	H	nd
			RT	I	H	H	H
			WH	I	H	L	nd
			MQ	L	H	L	H
–OH	Hydroxyl	3250–3650, 1400–1450, 1000–1050	CR	H	H	L	nd
			RT	I	H	nd	nd
			WH	I	H	L	nd
			MQ	M	H	M	H
$–NH_2$	Amino	3300–3500, 1550–1650, 660–900	CR	M	H	L	nd
			RT	L	H	H	nd
			WH	M	H	M	H
			MQ	M	H	M	H
–CO	Carbonyl carbons	1640–1850	CR	Nd	H	L	H
			RT	L	H	nd	H
			WH	nd	H	M	H
			MQ	I	nd	M	H

*particle size range of > 1.8 µm was considered as coarse particles for qualitative analysis;
**particle size range of 1–1.8 µm was considered as intermodal particles for qualitative analysis; Occurrence frequency High, H: > 75%; Moderate, M: 50–75%; Intermediate, I: 25–50%; Low, L: < 25%, and nd: not detected.

2850 cm^{-1} (Table 2, Fig. 3) is attributed to $–CH_2$ asymmetric vibration. In addition, the absorption at 1410 cm^{-1} is assigned to the bending vibration with $–CH_2$ deformation, which indicates the organic compound could originate from aliphatic compounds (Coates, 2000). This aliphatic carbon bond was identified in the atmospheric particle size ranges from 0.18–10 μm at all four sampling sites. The stretching vibration at 2850–3000 cm^{-1} was selected for the relative quantification of the $–CH_2$ group.

Hydroxyl (–OH) Group

Hydroxyl group mainly occurs at the 3250–3650 cm^{-1} absorption range. Moderate to strong, and broad stretching vibrations were observed at 3350 and 3390 cm^{-1} in this study (Table 2, Fig. 3) which may be depicted as free OH and hydrogen bonding of an alcohol functional group (Coates, 2000) in addition to the IR bands of surface OH on crystals and salt hydrates. Moderate bending vibrations were also found in the region of 1400–1450 and 1000–1050 cm^{-1} which can be assigned to OH bending of phenol or tertiary alcohol (Coates, 2000). Thus, aromatic compounds with OH groups, such as phenol, could exist in atmospheric particles. From the structural point of view, these alcohols may be derived by replacing the H–atoms from a parent water molecule by a C–based alkyl group. The structural modification of organic compounds, such as alcohol and ether, may also result in significant changes in physical and chemical properties of these compounds, depending on their hydroxyl content and ability to participate in the H–bonding. The surfaces of crystals are also covered with hydroxyl groups, the vibration of which may appear at 3250–3650 cm^{-1}. For example, goethite (FeO_2H) shows –OH vibration

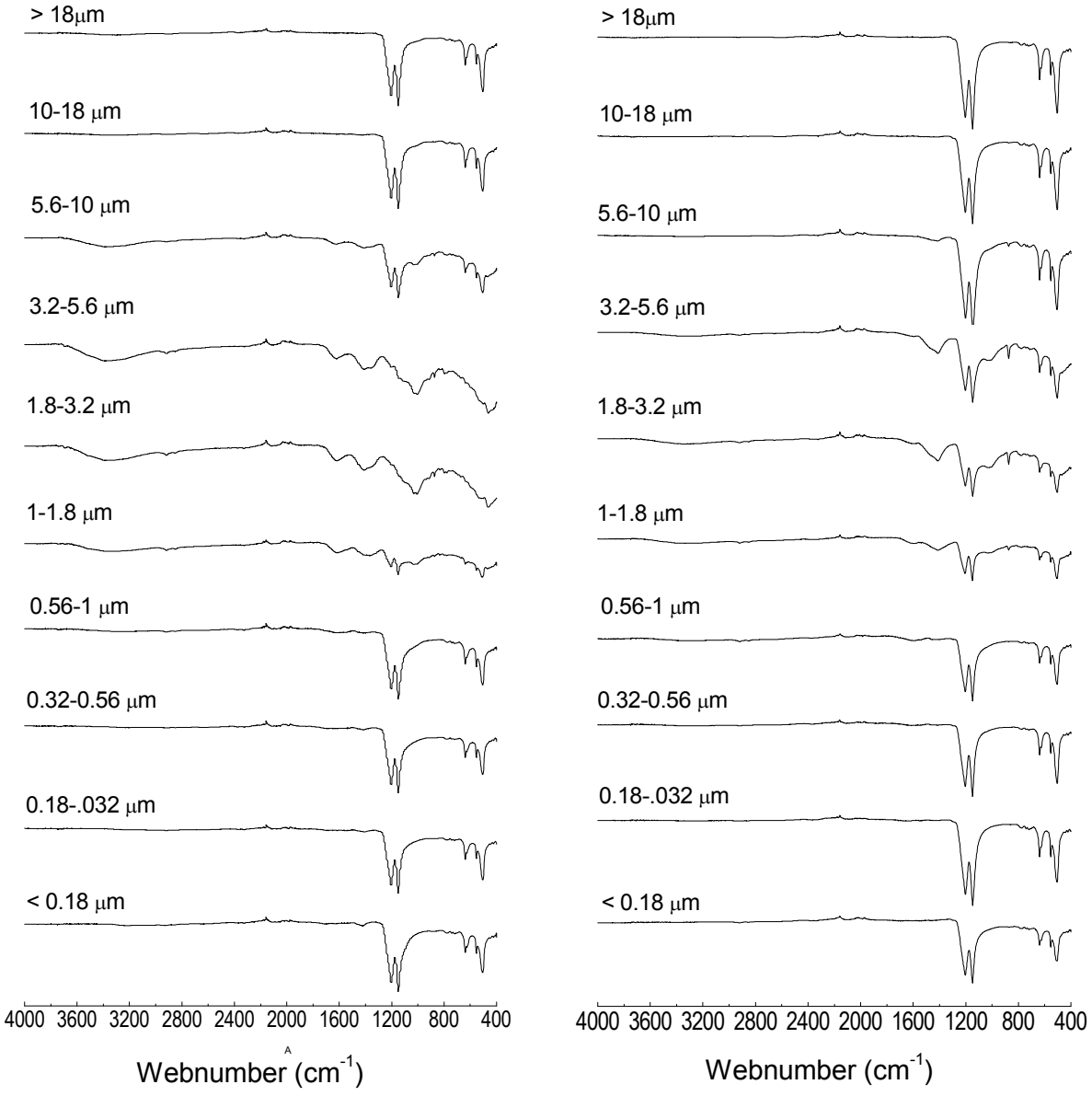

Fig. 3. FTIR scans for size resolved aerosol samples at CR and RT sites.

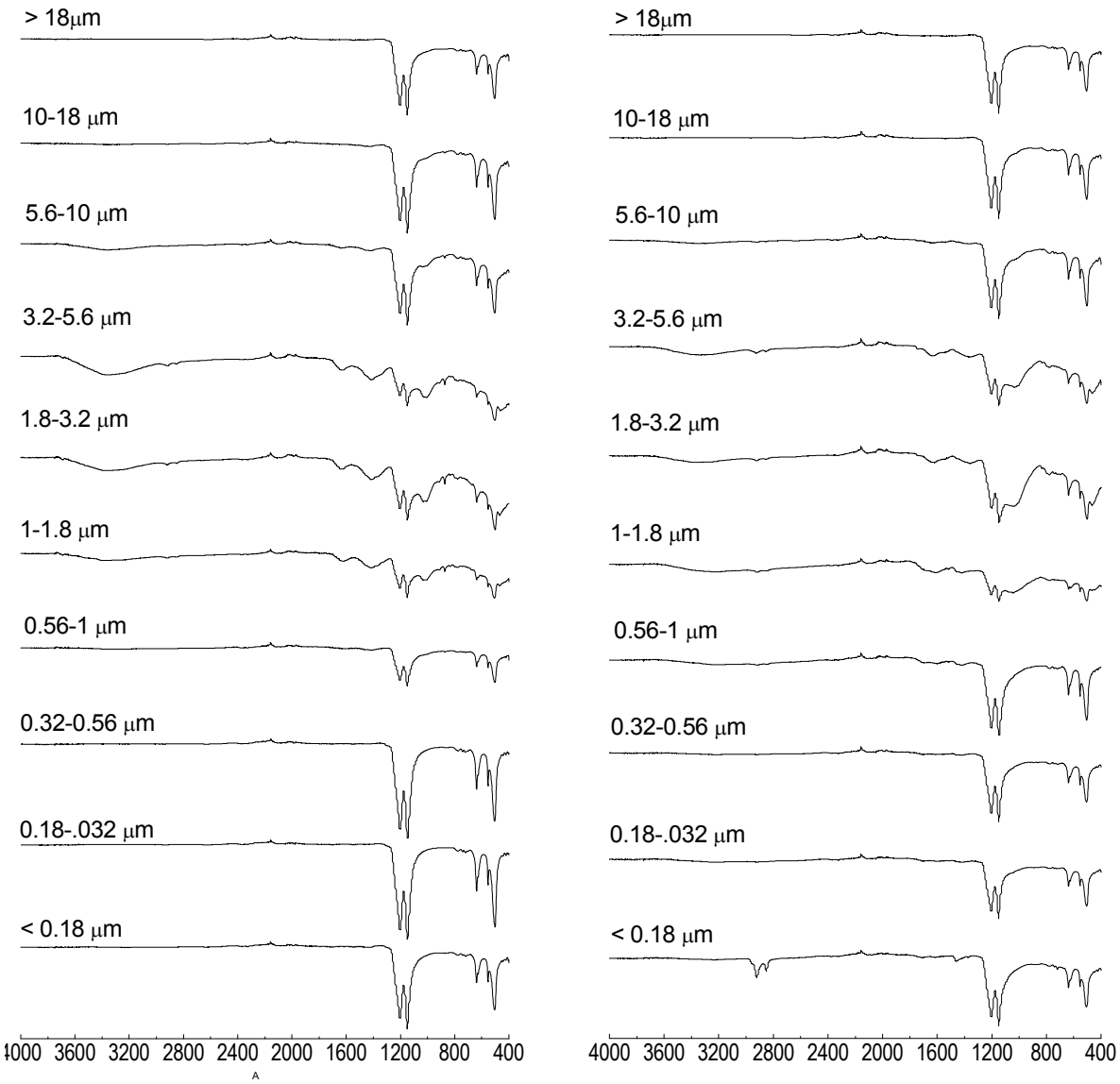

Fig. 3. (*continued*).

band at 3484 cm^{-1} (Cornell and Schwertmann, 2006). Furthermore, the –OH stretch vibrations were reported for hematite (Fe_2O_3), although hematite contained no structural OH groups (Rochester and Topham, 1979). Goethite was detected in the atmospheric particles sampled at the CR and WH sites while hematite was detected in the atmospheric particles sampled at the CR, RT and WH sites (Table 3). In addition, water strongly adsorbed on aerosol salts absorbs at 1600–1700 cm^{-1} and broadly at 3100–3600 cm^{-1} (Allen, 1994). Halite was detected in the atmospheric particles sampled at the CR, RT and MQ sites (Table 2). This hydroxyl bond was mainly observed in the particle size ranges of 1–18 μm at all studied sites. The vibrations at 3250–3650 cm^{-1} were used to calculate the relative quantity of organic –OH group in the atmospheric particles by subtracting fraction of inorganic –OH groups from goethite (FeO_2H) and halite.

Amino (–NH_2) Group

Amino (–NH_2) group is regarded as an amino substituent derived from ammonia (NH_3), and has similar sp^3 structural features. Amino (–NH_2) group can occur in different vibrations from 3300–3500, 1550–1650 and 660–900 cm^{-1}. It appears that weak N–H bond overlapped and disappeared when the strong O–H bond was identified in 3300–3500 cm^{-1}. The medium to strong bending vibration at 1621 cm^{-1} (Table 2, Fig. 3) was attributed to the –NH_2 scissoring, and vibration at 873 cm^{-1} was assigned to NH_2 wagging, indicating these organic compounds may originate from the primary amino compounds in addition to the IR bands of organonitrates, such as $RONO_2$, which may also absorb around 1631 cm^{-1} (Allen *et al.*, 1994). Organonitrates are expected to contribute for the secondary organic aerosol formation. This group was mainly observed in the particle size range of 0.56–10 μm at

all four sampling sites. The bending vibration at 1600–1660 cm^{-1} was selected for relative quantification of the organic $–NH_2$ group by subtracting the relative contribution of organonitrates in atmospheric particles (≤ 0.1 μm).

Carbonyl (–CO) Group

The structural features of the carbonyl group can be found in several classes of organic compounds which impose very specific planar geometry associated with sp2 hybridised carbon and oxygen, such as aldehyde (R–COH), ketone (R–CO–R) and carboxylic acid (R–COOH). This group can blend with other functional groups resulting in properties and reactivities of combined functional groups. Carbonyl group can appear in a broad frequency range of 1640–1850 cm^{-1} (Table 2, Fig. 3) with specific peaks from low to high frequencies depending on various functional groups from amide to open-chain acid anhydride. The absorption bands found at 1794 cm^{-1}, 1714 cm^{-1}, and 1695 cm^{-1} match well with the reactive carbonyl compound (acid halide and aryl carbonate), simple carbonyl compound (ketone) and conjugated carbonyl compound (conjugated ketone), respectively, (Coates, 2000) in the particle sizes below 1.8 μm for all four sampling sites. The vibration at 1680–1720 cm^{-1} was assigned to the relative quantification of –CO group.

Functional Group Distribution

The strength, occurrence and modality type of functional groups, are essential to understand the behaviour of organic compounds in atmospheric particles, which are independent of the calibration value. Fig. 4 shows the distribution of hydroxyl, aliphatic carbon, carbonyl and amino functional groups in the size resolved atmospheric particles collected from the four sampling sites. Functional group distribution as a function of particle size revealed that elevated level was found for –OH, –CO and $–NH_2$ groups at CR and MQ sites, and $–CH_2$ group at RT and MQ sites. The functionality distribution was found variable between mass and bonding groups, among bonding groups, and among urban and industrial areas. Single mode distribution was found predominantly in –OH, $–CH_2$, –CO, and $–NH_2$ groups at all three industrial CR, RT, and WH sites whereas bimodal distribution was observed for –OH, $–CH_2$, and –CO groups at the urban background MQ site. The high absorption peak occurred in the particle size range of 1.4–4.4 μm (–OH), 0.78–1.4 μm ($–CH_2$), 0.10–0.78 μm (–CO), and 0.78–4.4 μm ($–NH_2$) (Fig. 4).

The hydroxyl (–OH) group (in alcohol compounds, surface OH on crystals, salt hydrate), aliphatic carbon ($–CH_2$) group (in methylene compounds, n-alkane), carbonyl (–CO) group (in acid halide, aryl carbonate, ketone, conjugated ketone), and amino ($–NH_2$) group (in primary amino compounds such as n-butylamine) in atmospheric particles in the industrial areas at the CR, RT and WH sites can be attributed to mainly anthropogenic sources, which include iron and steelmaking industries (Environment Protection Authority, 2013) and motor vehicles exhaust (Schauer and Cass, 2000; Xie *et al.*, 2009). These compounds can also originate from long range transport particles (Radhi *et al.*, 2010), microbiological processes of biogenic sources (Kavouras *et al.*, 1999) and wood heaters (Environment Protection Authority, 2013), especially in the winter period. The increasing amount of organic compounds in atmospheric particles in the urban background site compared to the industrial sites (Fig. 4) may be due to the strong influence of local biogenic emissions of isoprene and pinenes due to long subsidence period (~72 hrs) leading to trapping of these particles from surrounding plants. The variation in bonding group distribution can also be influenced by atmospheric conditions and formation of secondary organic aerosols by atmospheric photochemical reactions.

Functional Groups Fraction

Fig. 5 shows the relative percentage of functional groups in the coarse, intermodal and submicron particles in urban and industrial areas. The –OH group is strongly associated with the coarse particles, which may suggest possible contribution of salt hydrate, such as halite, at CR, WH, and MQ sites, and surface OH on crystals, such as goethite, at CR and WH sites, whereas the $–CH_2$ group is associated with intermodal particles (at WH site) and submicron particles (at RT site). The salt hydrate in atmospheric particles could originate from sea spray and long-range transport particles (Radhi *et al.*, 2010). The back trajectories of WH and MQ sampling sites using HYSPLIT model, shown in Fig. 2, also indicate the contribution of halite from the ocean. The –CO group is predominantly associated with submicron particles at all sampling sites. The $–NH_2$ group is found substantial with submicron particles (at RT site), and intermodal particles (at WH site). The strong association of bonding groups with submicron particles may be associated to the vehicle exhaust, and secondary organic particles from atmospheric photochemical reactions.

XRD ANALYSIS

Mineral Identification and Composition

The XRD analysis was performed on the atmospheric particles (0.10 < Dp < 18 μm), and the dominant minerals of quartz (SiO_2), hematite (α-Fe_2O_3), calcite ($CaCO_3$), goethite (FeO_2H), magnetite (Fe_3O_4), halite (NaCl), maghemite (γ-Fe_2O_3), ilmenite ($FeTiO_3$), and franklinite ($ZnFe_2O_4$) were identified in the inorganic fraction of the samples. Fig. 6 shows the typical XRD pattern of the size resolved atmospheric particles in one of the industrial (WH) sites. Fe-containing minerals (hematite, goethite, magnetite, maghemite, ilmenite and franklinite) dominate the atmospheric particles in the vicinity of iron and steelmaking industries at the CR, RT, and WH sites, whereas the background MQ site contained primarily quartz, calcite, and halite. Calcite minerals can originate from steelmaking sources, as they are used as fluxing agents, in addition to the natural mineral sources. Halite could originate from the sea spray at the CR, WH, and MQ sites; however the RT site was not influenced by the halite minerals, possibly due to the prevailing atmospheric conditions and further distance from the ocean, comparable to the other three sites. Iron titanium oxide ($FeTiO_3$), and franklinite ($ZnFe_2O_4$) were found at the RT site where electric arc furnace steelmaking processes are

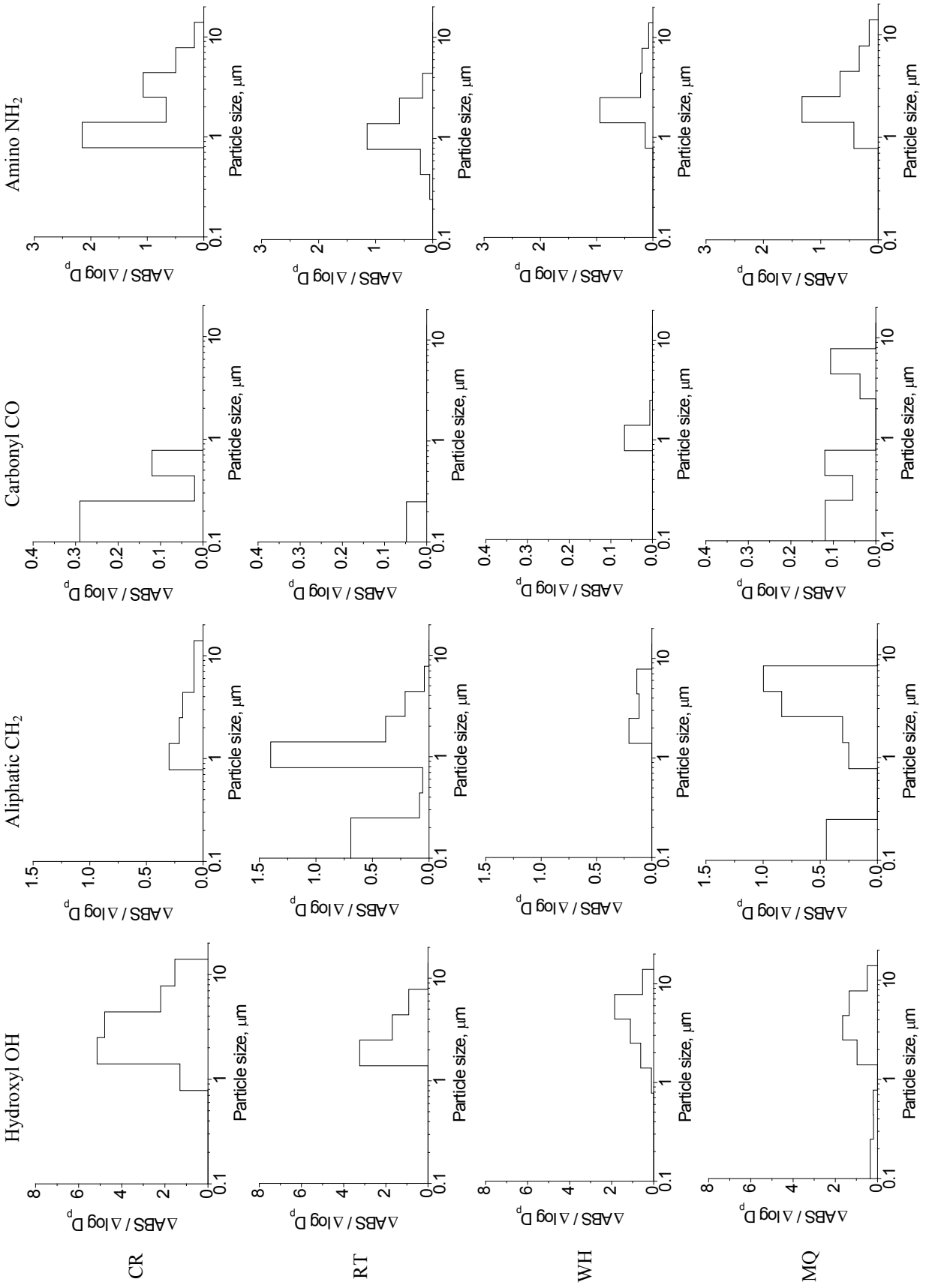

Fig. 4. Functional group distribution as a function of particle size at CR, RT, WH and MQ sites.

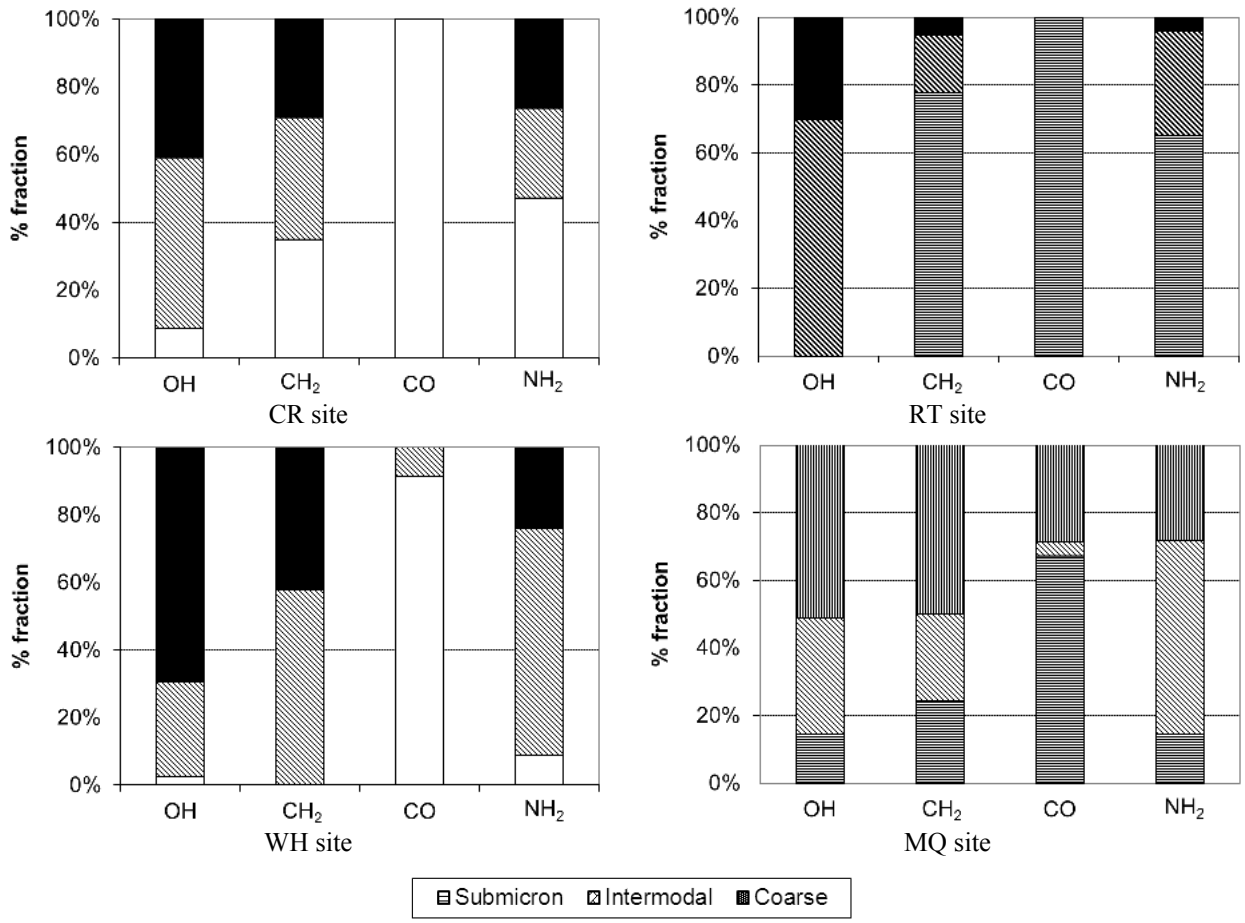

Fig. 5. Coarse, intermodal and submicron PM functional group fractions.

operating. Maghemite was found at the WH site where integrated BF-BOF steelmaking process is operating, and the surrounding soils also contain a variety of iron minerals.

Table 3 shows the mineral content (in percentage) of size resolved atmospheric particles considering total crystalline materials found in the particles apart from the amorphous materials. For this, the mineral content (Table 3) represents the relative percentage among all minerals identified and quantified in a particular atmospheric particle sample. It is observed that the increasing percentage in the different particle size fractions does not necessarily indicate the higher mineral mass. For example, hematite is found in S2 stage (26%), and S5 stage (79%) at the WH site, but the mass concentration of hematite might be higher in the S2 stage compared with the S5 stage. The relative mineral content can be discussed and compared based on the total crystalline materials in each sample set to 100%, regardless of their mass concentration. Hence, careful consideration is necessary for reporting the mineral quantification, especially for the size resolved atmospheric particles. Ohmsen (2004b) reported that air-fall dust at Whyalla Wall Street contains about 18–45% hematite, however, these values represent the percentage hematite content in total crystalline materials where the mass of total crystalline materials is unknown. In this case, the lower percentage of mineral content may represent higher significance in terms of their implication and effect on human health and the environment.

The results of the XRD analysis of size resolved atmospheric particles (Table 3) showed the abundance of quartz, calcite, halite and hematite minerals. Hematite was found dominant mineral in the vicinity of iron and steelmaking sites (CR, RT and WH sites), whereas the background MQ site contained quartz, calcite and halite minerals, most likely from the natural soil dust and sea spray. Apart from hematite minerals, a considerable amount of goethite, magnetite, iron titanium oxide, franklinite and maghemite were found nearby the steelmaking industrial sites, indicating strong influence of iron and steelmaking processes on surrounding atmospheric particle mineralogy.

At stages S0–S1 (> 10 μm) halite (up to 91%) was found dominant at the background MQ site. Calcite (up to 38%) and quartz (up to 80%) minerals were found at all sampling sites. The Fe-minerals hematite (up to 76%), goethite (2%) and magnetite (11%) were dominant at the WH site, indicating the increasing amount of iron crystalline materials originating from raw materials handling. At stages S2–S4 (1.8–10 μm) the atmospheric particles contained both background and iron bearing minerals. These stages are particularly important as the dominant mass and elemental concentration occurred within these particle sizes at all sampling sites. The iron bearing minerals at the RT site contained hematite (up to 17%), goethite (11%), ilmenite

Q: quartz; C: calcite; H: hematite; M: magnetite; Mm: maghemite; L: halite; G: goethite; T: Teflon substrate

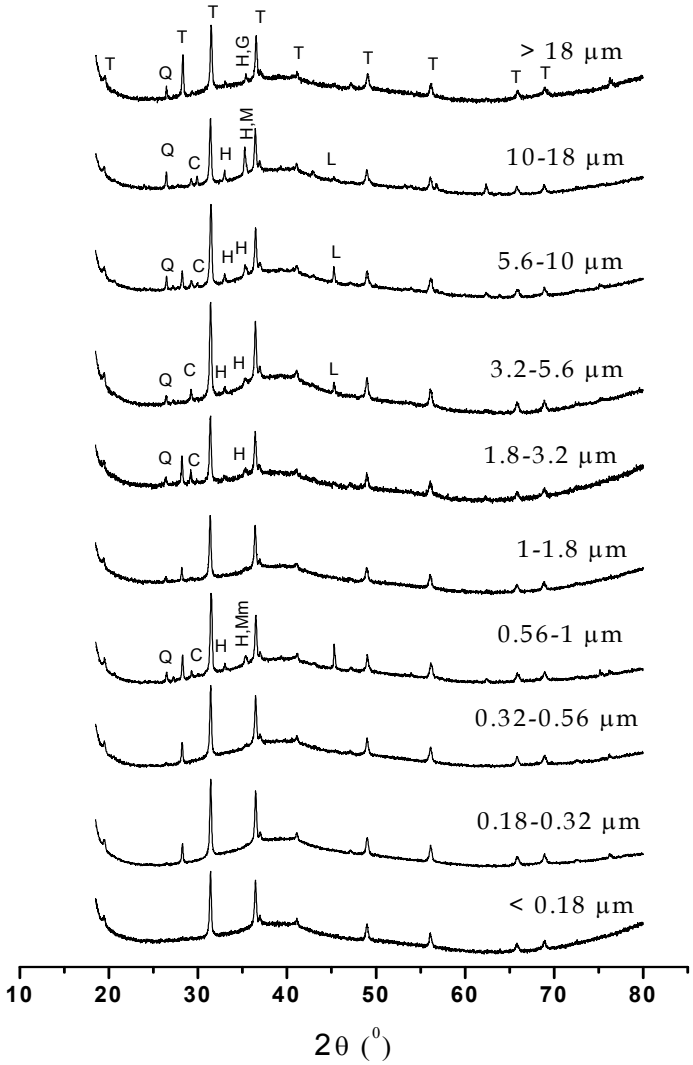

Fig. 6. Typical XRD diffraction pattern of size resolved atmospheric particles at WH site.

(50%), franklinite (up to 40%) and magnetite (14%) minerals, which shows the diverse crystalline materials originated from electric arc furnace (EAF) steelmaking processes compared to blast furnace-basic oxygen furnace (BF-BOF) steelmaking processes. Hematite was absent at the background MQ site, indicating the importance of distance between industries and receptor sites on the composition of the surrounding atmospheric particles. Halite (up to 72%), quartz (up to 16%), and calcite (up to 35%) were found in the particle size range of 1.8 – 10 µm at all sampling sites. At stages S5–S7 (0.32–1.8 µm) halite crystal phase was absent at all sampling sites. Fe-containing minerals at WH site constituted of hematite (up to 79%), and maghemite (up to 84%). The mass concentration in these particle sizes was found to be substantially lower compared to coarse particles. Among the crystalline materials, hematite (up to 99%) was found predominantly at the RT site, whereas both hematite (up to 68%), and goethite (up to 16%) were found significant at the CR site. At stages S8-SP (< 0.32 µm) minerals are not detected in most samples, possibly due to the lower concentration of crystalline materials in these particle sizes.

The variation in the crystalline phases and their contents in industrial atmospheric particles could result from a number of factors, such as the distance between the industrial sources and receptor sites, prevailing atmospheric conditions including wind speed and direction, raw materials variation in EAF and BF–BOF steelmaking processes, processing variations, such as pellet plants at WH site and sinter plant at CR site, the production and variability of emissions from iron and steelmaking point sources. The overall crystalline phases show the dominant iron crystalline materials originate from fugitive and point sources at the steelmaking sites CR, RT, and WH. The fugitive emissions can be reduced significantly by introducing advanced dust free raw materials

Table 3. Mineral content (%) as a function of total crystalline materials in size resolved atmospheric particles at CR, RT, WH, and MQ sites.

Stage no	Particle Size, μm	Site	Quartz	Hematite	Calcite	Goethite	Halite	Iron titanium oxide	Franklinite	Magnetite	Maghemite
S0	> 18	CR	80				20				
		RT	39	24	38						
		WH	21	76	1	2					
		MQ	9				91				
S1	10–18	CR	12	42	29		17				
		RT	39	32	28						
		WH	21	21	15		32			11	
		MQ	14		23		64				
S2	5.6–10	CR	10	21	33		36				
		RT	15		35			50			
		WH	16	26	29		30				
		MQ	15		13		72				
S3	3.2–5.6	CR	9	34	21	11	25				
		RT	15	17	28				40		
		WH	14	17	14		55				
		MQ	4		24		72				
S4	1.8–3.2	CR	10	53	13		24				
		RT	18	17	26				25	14	
		WH	14	16	21		49				
		MQ	9		29		63				
S5	1–1.8	CR	8	51	42						
		RT	20	57	2				21		
		WH	10	79	1						11
		MQ	43		58						
S6	0.56–1	CR	13	87							
		RT		92						2	
		WH	16								84
		MQ	54		46						
S7	0.32–0.56	CR		68	20	13					
		RT		99						1	
		WH	24								76
		MQ	nd								
S8	0.18–0.32	CR		58	26	16					
		RT		99						1	
		WH	nd								
		MQ	nd								
SP	< 0.18	CR	nd								
		RT	nd								
		WH	nd								
		MQ	nd								

nd: not detected.

handling operations. The Fe-nanocrystalline phases in atmospheric particles (γ-Fe_2O_3 or Fe_3O_4 nanocrystals of approximately 10 nm in size) (Tartaj *et al.*, 2004; Ge *et al.*, 2007), could be generated from high temperature combustion processes in iron and steelmaking industries, but in this study they were mostly not detected, likely due to the insufficient amount of crystalline material present in the inorganic compounds of the ultrafine particles. The dominance of iron minerals, especially hematite, in the vicinity of iron and steelmaking industries showed the importance of mineral analysis for anthropogenic contribution to the radiative forcing of atmospheric particles.

CONCLUSIONS

Bonding structure and mineral content of atmospheric particles in the vicinity of Australian electric arc furnace and integrated steelmaking industries were investigated in

this work, focusing on different size fractions from coarse to ultrafine particles for improved understanding of radiative forcing of atmospheric particles. The hydroxyl (–OH) group (in alcohol compounds, surface OH on crystals, salt hydrate), aliphatic carbon ($–CH_2$) group (in methylene compounds, n-alkane), carbonyl (–CO) group (in acid halide, aryl carbonate, ketone, conjugated ketone) and amino ($–NH_2$) group (in primary amino compounds such as n-butylamine) in atmospheric particles at all sampling sites were detected in this study. The functional group distributions were found variable between mass and bonding groups, among bonding groups, and among urban and industrial areas. These functional groups in organic compounds at the three industrial sites can be attributed to the influence of iron and steelmaking industries and motor vehicle exhaust, whereas strong influence of organic functional groups at the urban background MQ site can be assigned to the local biogenic emissions. The –OH group was mostly associated with coarse particles, whereas $–CH_2$, –CO, and $–NH_2$ groups were mostly associated with submicron particles, indicating strong influence of fine particle sources of combustion process, car exhaust, domestic wood burning and biogenic emissions. Hematite mineral was found predominantly in the vicinity of iron and steelmaking industries, which likely originates from the raw materials handling and high temperature combustion processes, whereas the background minerals, such as quartz, calcite and halite, were found predominantly at the urban background site. The nanocrystalline iron minerals in ultrafine particles were not detected, which requires further investigation for comprehensive understanding of the atmospheric particle characterisation. The presence of hematite content as major mineral species can provide improved understanding of radiative forcing of the mineral component of atmospheric particles.

ACKNOWLEDGMENTS

The authors acknowledge and are grateful for the financial support from the Australian Research Council (grant no. LP11020063), and Macquarie University Research Office (grant no. HDR40940155). The authors also acknowledge Mr. Russell Field and Professor Damian Gore for their support with XRD laboratory analysis at Macquarie University.

REFERENCES

Alcock, R.E. (2003). *Health risks of persistent organic pollutants from long-range transboundary air pollution.* Joint WHO/Convention Task Force on the Health Aspects of Air Pollution.

Allen, D.T., Palen, E.J., Haimov, M.I., Hering, S.V. and Young, J.R. (1994). Fourier transform infrared spectroscopy of aerosol collected in a low pressure impactor (LPI/FTIR): Method development and field calibration. *Aerosol Sci. Technol.* 21: 325–342.

Braakhuis, H.M., Park, M.V., Gosens, I., De Jong, W.H. and Cassee, F.R. (2014). Physicochemical characteristics of nanomaterials that affect pulmonary inflammation. *Part. Fibre Toxicol.* 11: 18.

Calvo, A., Alves, C., Castro, A., Pont, V., Vicente, A. and Fraile, R. (2013). Research on aerosol sources and chemical composition: Past, current and emerging issues. *Atm. Res.* 120: 1–28.

Claquin, T., Schulz, M. and Balkanski, Y. (1999). Modeling the mineralogy of atmospheric dust sources. *J. Geophys. Res.* 104: 22243–22256.

Coates, J. (2000). Interpretation of infrared spectra, a practical approach. In *Encyclopedia of Analytical Chemistry,* Meyers, R.A. (Ed.), John Wiley & Sons Ltd, Chichester, pp. 10815–10837.

Cohen, D., Stelcer, E., Atanacio, A. and Crawford, J. (2014). The application of IBA techniques to air pollution source fingerprinting and source apportionment. *Nucl. Instrum. Methods Phys. Res., Sect. B* 318: 113–118.

Cornell, R.M. and Schwertmann, U. (2006). *The iron oxides: structure, properties, reactions, occurrences and uses*, John Wiley & Sons.

Coury, C. and Dillner, A.M. (2008). A method to quantify organic functional groups and inorganic compounds in ambient aerosols using attenuated total reflectance FTIR spectroscopy and multivariate chemometric techniques. *Atmos. Environ.* 42: 5923–5932.

Coury, C. and Dillner, A.M. (2009). ATR-FTIR characterization of organic functional groups and inorganic ions in ambient aerosols at a rural site. *Atmos. Environ.* 43: 940–948.

Cupr, P., Flegrová, Z., Franců, J., Landlová, L. and Klánová, J. (2013). Mineralogical, chemical and toxicological characterization of urban air particles. *Environ. Int.* 54: 26–34.

Dockery, D.W., Pope, C.A., Xu, X., Spengler, J.D., Ware, J.H., Fay, M.E., Ferris Jr, B.G. and Speizer, F.E. (1993). An association between air pollution and mortality in six US cities. *N. Engl. J. Med.* 329: 1753–1759.

Ehn, M., Thornton, J.A., Kleist, E., Sipilä, M., Junninen, H., Pullinen, I., Springer, M., Rubach, F., Tillmann, R. and Lee, B. (2014). A large source of low-volatility secondary organic aerosol. *Nature* 506: 476–479.

Environment Protection Authority (2013). Managing particles and improving air quality in NSW. EPA NSW, Sydney.

Ge, J., Hu, Y., Biasini, M., Beyermann, W.P. and Yin, Y. (2007). Superparamagnetic magnetite colloidal nanocrystal clusters. *Angew. Chem. Int. Ed.* 46: 4342–4345.

Ghauch, A., Deveau, P.A., Jacob, V. and Baussand, P. (2006). Use of FTIR spectroscopy coupled with ATR for the determination of atmospheric compounds. *Talanta* 68: 1294–1302.

Hallquist, M., Wenger, J., Baltensperger, U., Rudich, Y., Simpson, D., Claeys, M., Dommen, J., Donahue, N., George, C. and Goldstein, A. (2009). The formation, properties and impact of secondary organic aerosol: current and emerging issues. *Atmos. Chem. Phys.* 9: 5155–5236.

Hibberd, M., Selleck, P., Keywood, M., Cohen, D., Stelcer, E. and Atanacio, A. (2013). Upper hunter particle characterisation study: Final report. CSIRO, Australia.

Hleis, D., Fernández-Olmo, I., Ledoux, F., Kfoury, A.,

Courcot, L., Desmonts, T. and Courcot, D. (2013). Chemical profile identification of fugitive and confined particle emissions from an integrated iron and steelmaking plant. *J. Hazard. Mater.* 250–251: 246–255.

Journet, E., Balkanski, Y. and Harrison, S. (2014). A new data set of soil mineralogy for dust-cycle modeling. *Atmos. Chem. Phys.* 14: 3801–3816.

Karlson, L., Greene, R., Scott, K., Stelcer, E. and O'loingsigh, T. (2014). Characteristics of aeolian dust across northwest Australia. *Aeolian Res.* 12: 41–46.

Kavouras, I.G., Lawrence, J., Koutrakis, P., Stephanou, E. G. and Oyola, P. (1999). Measurement of particulate aliphatic and polynuclear aromatic hydrocarbons in Santiago de Chile: source reconciliation and evaluation of sampling artifacts. *Atmos. Environ.* 33: 4977–4986.

Lu, S., Luan, Q., Jiao, Z., Wu, M., Li, Z., Shao, L. and Wang, F. (2007). Mineralogy of inhalable particulate matter (PM_{10}) in the atmosphere of Beijing, China. *Water Air Soil Pollut.* 186: 129–137.

Maria, S.F., Russell, L.M., Turpin, B.J. and Porcja, R.J. (2002). FTIR measurements of functional groups and organic mass in aerosol samples over the Caribbean. *Atmos. Environ.* 36: 5185–5196.

Meland, B., Kleiber, P., Grassian, V. and Young, M. (2011). Visible light scattering study at 470, 550, and 660nm of components of mineral dust aerosol: Hematite and goethite. *J. Quant. Spectrosc. Radiat. Transfer* 112: 1108–1118.

Mohiuddin, K., Strezov, V., Nelson, P. and Stelcer, E. (2014a). Characterisation of trace metals in atmospheric particles in the vicinity of iron and steelmaking industries in Australia. *Atmos. Environ.* 83: 72–79.

Mohiuddin, K., Strezov, V., Nelson, P.F., Stelcer, E. and Evans, T. (2014b). Mass and elemental distributions of atmospheric particles nearby blast furnace and electric arc furnace operated industrial areas in Australia. *Sci. Total Environ.* 487: 323–334.

Ohmsen, G. (2004a). *Characterisation and source apportionment of air-fall dusts, Whyalla*. Department of Health, South Australia.

Ohmsen, G. (2004b). Quantitative X-Ray diffraction and chemical analysis of TSP and PM_{10} filters collected from hummock hill, walls street and Civic Park, Wyalla. Department of Health, South Australia.

Radhi, M., Box, M., Box, G., Mitchell, R., Cohen, D., Stelcer, E. and Keywood, M. (2010). Size-resolved mass and chemical properties of dust aerosols from Australia's Lake Eyre Basin. *Atmos. Environ.* 44: 3519–3528.

Reynolds, R.L., Cattle, S.R., Moskowitz, B.M., Goldstein, H.L., Yauk, K., Flagg, C.B., Berquó, T.S., Kokaly, R.F., Morman, S. and Breit, G.N. (2014). Iron oxide minerals in dust of the Red Dawn event in eastern Australia, September 2009. *Aeolian Res*. 15: 1–13.

Rochester, C.H. and Topham, S.A. (1979). Infrared study of surface hydroxyl groups on haematite. *J. Chem. Soc., Faraday Trans. 1* 75: 1073–1088.

Roos, G. (1997). *Organic chemical concepts*, Harcourt Brace & Company, Marrickville, NSW.

Schauer, J.J. and Cass, G.R. (2000). Source apportionment of wintertime gas-phase and particle-phase air pollutants using organic compounds as tracers. *Environ. Sci. Technol.* 34: 1821–1832.

Shah, P.S. and Balkhair, T. (2011). Air pollution and birth outcomes: A systematic review. *Environ. Int.* 37: 498–516.

Sokolik, I.N. and Toon, O.B. (1999.) Incorporation of mineralogical composition into models of the radiative properties of mineral aerosol from UV to IR wavelengths. *J. Geophys. Res.* 104: 9423–9444.

Tartaj, P., Gonzalez-Carreno, T., Bomati-Miguel, O., Serna, C. and Bonville, P. (2004). Magnetic behavior of superparamagnetic Fe nanocrystals confined inside submicron-sized spherical silica particles. *Phys. Rev. B* 69: 094401.

Xie, M., Wang, G., Hu, S., Han, Q., Xu, Y. and Gao, Z. (2009). Aliphatic alkanes and polycyclic aromatic hydrocarbons in atmospheric PM_{10} aerosols from Baoji, China: Implications for coal burning. *Atmos. Res.* 93: 840–848.

Received for review, July 7, 2015
Revised, November 10, 2015
Accepted, December 17, 2015